Continuum Mech. Thermodyn. (2019) 31:209–223
https://doi.org/10.1007/s00161-018-0678-y

ORIGINAL ARTICLE

Emilio Turco · **Anil Misra** · **Rizacan Sarikaya** · **Tomasz Lekszycki**

Quantitative analysis of deformation mechanisms in pantographic substructures: experiments and modeling

Received: 5 December 2017 / Accepted: 3 May 2018 / Published online: 17 May 2018

Abstract In order to get detailed information about the mechanical behavior of pantographic elementary substructure and elements, small-scale specimens were sintered using polyamide powder, constituted by three orthogonal pairs of beams interconnected through pivots forming pantographic cells. The mechanical properties of interconnecting pivots and constituting beams are investigated by comparing experimental evidence with an enhanced Piola–Hencky model. The careful agreement between experimental and predicted results allows us to estimate: (i) the macro-shear stiffness of interconnecting pivots (corresponding to micro-torsional stiffness), (ii) extensional stiffness and (iii) bending stiffness of constituting beams.

Keywords Pantographic sheets · Discrete models · Nonlinear analysis

1 Introduction

Pantographic sheets have been primarily studied in the recent past few years, see e.g., [1–7], for their relevant technical applications. A key characteristic of these sheet structures is their capability to extend the elastic range of the used material to strain values close to 1. From the viewpoint of mathematical modeling, the mechanical behavior of these structures can be investigated via, broadly speaking, the following three approaches, each one having its own peculiarities and strengths:

Communicated by Francesco dell'Isola.

E. Turco (✉)
Department of Architecture, Design and Urban planning (DADU), University of Sassari, Sassari, Italy
E-mail: emilio.turco@uniss.it

A. Misra
Civil, Environmental and Architectural Engineering (CEAE), The University of Kansas, Lawrence, USA
E-mail: amisra@ku.edu

R. Sarikaya
Mechanical Engineering (ME), The University of Kansas, Lawrence, USA
E-mail: rsarikaya@ku.edu

T. Lekszycki
Warsaw University of Technology, Warsaw, Poland

T. Lekszycki
Department of Experimental Physiology and Pathophysiology, Medical University of Warsaw, Warsaw, Poland
E-mail: t.lekszycki@wip.pw.edu.pl

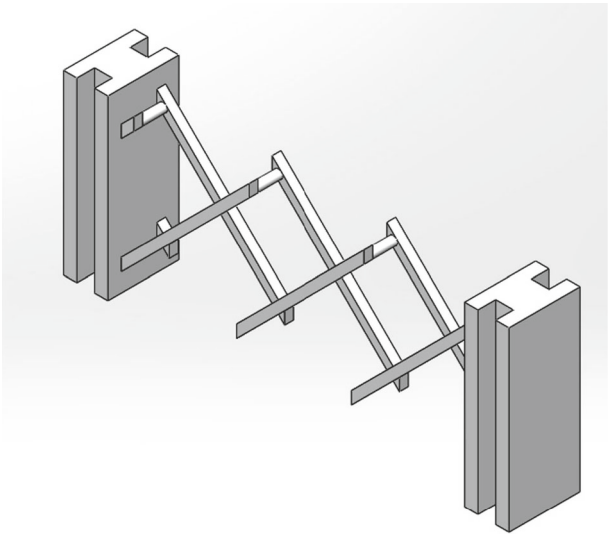

Fig. 1 Mini pantographic lattice: three-dimensional rendering

1. continuum, see, e.g., [8–27];
2. discrete, see, e.g., [28,29];
3. experimental using the potentialities of 3D printing process, see [30].

In addition, very recently, a comparison of the three aforementioned approaches have been initiated, see [31–33], where continuum and discrete models have been compared and their results validated by using experimental results. We remark that until some years ago, a large part of the published technical articles were devoted to continuum models which in order to treat problems of practical interest have to be discretized in any case.

Common to both continuum and discrete investigation approaches, there is the necessity to estimate the constitutive parameters relevant to the two kinds of models. There have been few attempts relative to the passage between the constitutive parameters for continuum and discrete models, or vice versa, as reported in [34–38]. Nevertheless, a satisfactory response to the following question remains to be given: how we can estimate the constitutive parameters for a continuum or discrete model starting from the results of physical experiments?

In order to proceed in the study of pantographic structures, and in particular to optimize their properties to particular applications, it is needed to identify the mechanical properties of each of its elementary components. Indeed, the overall properties of considered metamaterial depend on their geometric microstructure but also on the mechanical properties of their elementary constituents.

Such constituents are the interconnecting pivots and the beams that form the two fibers constituting the cell of the pantographic sheet (see the three-dimensional rendering reported in Fig. 1). The technical drawing shown in Fig. 2 furnishes the geometric data which characterize the mini pantograph. In addition, the micro-beams have a square cross section with side equal to 1 mm and the pivots are cylinders having height equal to 2 mm and circular cross section with a diameter of 0.9 mm.

The printed pantographic sheet along with left and right support are displayed in Fig. 3 at the beginning of the traction test by using the device ElectroForce 3200 (Bose, now TA Instruments). A load cell with capacity ± 22 N, a measurement uncertainty of 0.1% and precision of 0.001 N was used for force measurement, while the displacement was measured with the in-built transducer with a range ± 6.5 mm, a measurement uncertainty of 0.1% and precision 0.001 mm.

Indeed, every pantographic substructure which we consider here one can distinguish mainly three deformation mechanisms: bending of beam segments of fibers, their extension and micro-torsion of interconnecting pivots. We neglect torsion deformability of the micro-beams and the flexural deformability of the pivots since both their sections have been designed to minimize those contributions in comparison with those considered as shown by the various experimental observations.

The problem which we address here is to determine experimentally:

(i) the macro-shear stiffness of interconnecting pivots (corresponding to micro-torsional stiffness) which are built as cylinders mechanically linking the two families of crossing fibers;

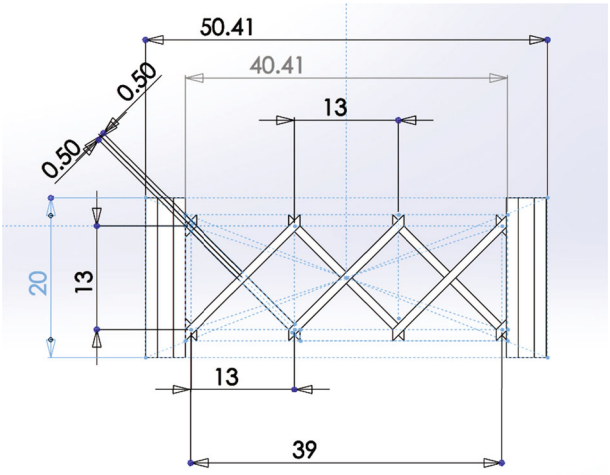

Fig. 2 Mini pantographic lattice: dimensioned drawing (in millimeters)

Fig. 3 Mini pantographic lattice in the testing machine

(ii) extensional stiffness of every beam segment of fiber mechanically linking the closest pairs of nodes, characterized as the sites where the pivots are located;
(iii) bending stiffness of aforementioned beam segments.

We believe, on the basis of observed breaking and failure phenomena, that the description of these three deformation mechanisms will also be useful to accurately describe the rupture mechanisms of pantographic sheets.

In the next sections, we first sketch an enhanced Piola–Hencky discrete model which is able to predict, when a suitable choice of its own constitutive parameters is used, the results of the physical experiment with a good degree of accuracy paying a reduced computational cost. Successively, we present and discuss some experimental results on the sheet formed by three orthogonal pairs of beams interconnected through pivots forming pantographic cells and their comparison with the results obtained by means of the enhanced Piola–Hencky discrete model. Finally, we sketch some concluding remarks along with some future challenges to tackle in future works.

2 Model and numerical aspects

2.1 Refined Piola–Hencky discrete model

A refinement of a completely discrete model for pantographic sheets (which undergo large displacements) has been previously introduced in [28] and exercised for several load conditions, see e.g., [31,32,39], and fiber orientations, see [33]. This refined model was conceived to improve the description of the strain energy related to the bending of the micro-beams. For the considered substructures, indeed, it is evident that the beam segment of fibers do bend between two nodes and that it is not possible to describe properly the corresponding bending energy solely with a elastic joint in correspondence of the pivot positions. The simplest way, if one wants to avoid the introduction of (more or less sophisticated) beam elements, is to introduce additional elastic joints between those already specified. In the jargon of finite elements this corresponds, roughly, to the so-called h-refinement.

By referring to Fig. 4 where three elastic joints (distinguished with a black bullet) are considered, namely P_{j-1}, P_j and P_{j+1} in the reference position (on the top) and by p_{j-1}, p_j and p_{j+1} in the actual position (on

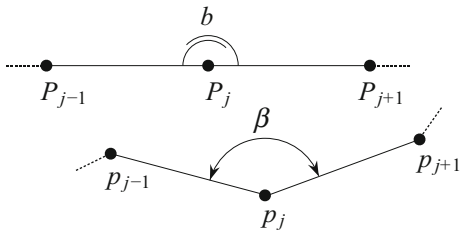

Fig. 4 Kinematic of a discrete beam model: reference (on the top) and current configuration (on the bottom)

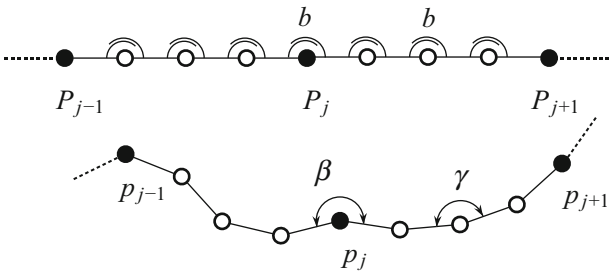

Fig. 5 Kinematic of the enhanced discrete beam model: reference (on the top) and current configuration (on the bottom)

the bottom), the bending strain energy contribution related to the elastic joint P_j is worth

$$E_{\mathrm{b}} = b\,(\cos\beta + 1)\,, \tag{1}$$

being b the bending stiffness of the elastic joints and β the angle between the rigid links p_{j-1}–p_j and p_j–p_{j+1}. The cosine of the angle β, which expresses the bending strain, can be easily computed, by means of the Carnot's theorem, making use of the coordinates of p_{j-1}, p_j and p_{j+1}, which is particularly effective when large displacements are considered.

A refined representation of the bending strain energy can be obtained by adding further elastic joints among those already mentioned, see Fig. 5, where these additional joints are represented as hollow bullets. In this way, we have also to consider the bending contributions related to the elastic joints both between P_{j-1} and P_j and between P_j and P_{j+1} (in Fig. 5, we have considered the case of three additional elastic joints between P_{j-1}–P_j and P_j–P_{j+1}) whose energy can be computed by using the same formula already introduced in Eq. (1) (In Fig. 5, we named as γ the angle, in the actual configuration, between the rigid links sharing the considered elastic joint).

The strain energy of the pantographic sheet model has to be completed adding, firstly, the stretching contribution of each micro-beam, as follows:

$$E_a = \frac{1}{2} a\,(\ell - \ell_0)^2\,, \tag{2}$$

where ℓ and ℓ_0 are the length of the micro-beam in the current and reference configuration, respectively, and a is its axial stiffness. In addition, we have to consider the shearing energy (for the two fibers which share the same pivot) stored as torsional energy in the small cylinders which connect non-parallel fibers (see Fig. 6), this energy can be written as:

$$E_{\mathrm{s}} = \frac{1}{2} \sum_{q=1}^{4} s \left(\sigma_q - \frac{\pi}{2}\right)^2, \tag{3}$$

where s is the shear stiffness of the considered elastic joint and σ_q the angle between two rigid links, in the actual position, in the qth quadrant ($q = 1, ..., 4$) (see Fig. 6 on the left). It is noted that, in this paper, we only consider the case of pantographic sheets with orthogonal fibers, although, see [33], it is convenient to remove this assumption.

The same expression for the shear energy can be used for the case of external pivots (those numbered with 4, 5, 7 and 8 in Fig. 7) only taking into account that in this case there is only one angle to consider (see again the sketch reported on the right part of Fig. 6).

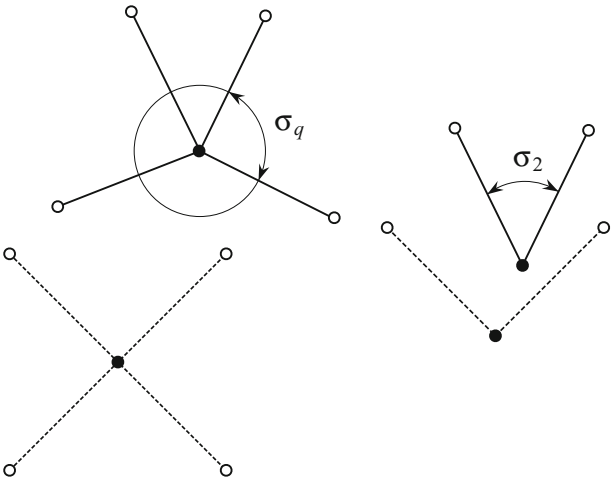

Fig. 6 Kinematic for internal, on the left, and external, on the right, pivots (reference and current configurations are depicted by using dashed and continuous lines, respectively)

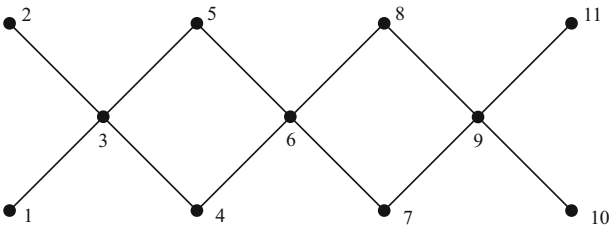

Fig. 7 Plane pantographic sheet model highlighting pivots

2.2 Numerical aspects: the arc-length method

The three strain energies immediately above described are the only quantities necessary to reconstruct the complete equilibrium path, that is the set of pairs $\{\lambda_i, \mathbf{u}_i\}$ where λ_i is a scalar parameter which control the external actions, i.e., load or given displacements, and $\mathbf{u}_i$ is the vector which collects the Lagrangian parameters which completely define the deformation, that is the displacements of elastic joints from the reference configuration. The strain energy of the whole pantographic structure E can be obtained simply by summing its elementary contributions using the elementary contributions given by (1), (2) and (3).

Since in this work we only consider problems where there are no external loads but only given displacements described by the form $\lambda\bar{\mathbf{u}}$ being $\bar{\mathbf{u}}$ a vector which collects the given displacements, therefore, the stationarity condition of the potential energy provides the nonlinear system of equations to solve:

$$\mathbf{s}(\mathbf{u}, \lambda\bar{\mathbf{u}}) = \nabla E = \mathbf{0}, \tag{4}$$

being $\mathbf{s}(\mathbf{u}, \lambda\bar{\mathbf{u}})$ the reaction depending both from the free displacements collected in $\mathbf{u}$ and the given displacements $\lambda\bar{\mathbf{u}}$. We remark that the reaction $\mathbf{s}$ can be obtained by assembling elementary contributions $\mathbf{s}_e$ defined as

$$\mathbf{s}_e = \frac{\mathrm{d}E_e}{\mathrm{d}\mathbf{u}_e}, \tag{5}$$

being E_e the elementary contribution to the strain energy (stretching, bending and shearing) and $\mathbf{u}_e$ the vector which collects the displacements of the nodes which contribute to the elementary strain energy, e.g., if the bending strain energy is considered, $\mathbf{u}_e$ collects the six displacements correspondent to three consecutive nodes.

In order to sketch a simple step-by-step strategy able to evaluate a point of the equilibrium path starting from the knowledge of the previous point, we need also the gradient of the reaction $\mathbf{s}$, in other words the tangent stiffness matrix $\mathbf{K}$:

$$\mathbf{K} = \nabla\mathbf{s} = \frac{\mathrm{d}\mathbf{s}}{\mathrm{d}\mathbf{u}}. \tag{6}$$

We remark that: *(i)* the given displacement $\lambda\bar{\mathbf{u}}$ has to be treated as known; therefore, $\mathbf{K}$ has the dimensions coherent with $\mathbf{u}$; *(ii)* exactly as for the reaction $\mathbf{s}$, the tangent stiffness matrix can be computed by assembling elementary contributions.

The solution of the nonlinear system of Eq. (4) can be found using a step-by-step algorithm based on the Newton's scheme. If the pair $\{\lambda_1, \mathbf{u}_1\}$ belongs to the equilibrium path, therefore its rest is zero, a nearby equilibrium point $\{\lambda_2, \mathbf{u}_2\}$ can be computed by means of the iterative scheme based on the first-order approximation of the rest, in much more simple terms *á la Newton*:

$$\Delta\mathbf{u} := \mathbf{u}_2 - \mathbf{u}_1 = -\mathbf{K}^{-1}\mathbf{s}\left(\mathbf{u}_1, (\lambda_1 + \Delta\lambda)\bar{\mathbf{u}}\right), \tag{7}$$

where $\Delta\lambda = \lambda_2 - \lambda_1$.

It is well known that Newton's scheme fails when the tangent stiffness matrix becomes singular and that this drawback can be overcome, using exactly the same tools already introduced, by using an arc-length strategy based on the Riks' idea [40]. Arc-length method was surely a keynote as proved by many papers populating technical references concerning changes, more or less important, of the same idea, see, for a comparison among different versions, the review paper [41]. In brief, the equilibrium curve is recovered using as parameter its arc-length and, therefore, no convergence problem arises when $\mathbf{K}$ becomes singular. A detailed description of an efficient implementation of the arc-length scheme can be found in [42] for problems which have to treat with limit points, e.g., to compute the limit load in perfect plasticity. In the following, we describe solution strategy for the case of given displacements since technical references treat almost exclusively problems with assigned external forces. Furthermore, we discuss some modifications devoted to improve the computational efficiency of the code.

The key point of the Riks' arc-length method is to describe the equilibrium curve using as parameter its arc-length (to describe the curve) instead of the non-dimensional given displacement λ and, therefore, to proceed for a fixed arc-length. Obviously, since we add a new unknown quantity (the arc-length parameter) a new equation has to be added. There are many possible choices which render the algorithm more or less complicated. The natural choice is to find the solution on the circle having as radius the arc-length even if this choice does not produce the faster algorithm. Much more simple to code, and more efficient from the computational point of view, is to impose a sort of orthogonality between the extrapolation and the correction that, in other words, is an approximate way to impose that the arc-length is constant.

The rest of the equilibrium equation (4), which should be zero when the convergence is achieved, can be written as:

$$\mathbf{s}\left(\mathbf{u}_1 + \Delta\mathbf{u} + \dot{\mathbf{u}}, \lambda_1 + \Delta\lambda + \dot{\lambda}\right) \approx \mathbf{0}, \tag{8}$$

being $\dot{\lambda}$ and $\dot{\mathbf{u}}$ the needed corrections to the extrapolations $\lambda_1 + \Delta\lambda$ and $\mathbf{u}_1 + \Delta\mathbf{u}$. Equation (8), using the analogous of Eq. (7), gives the free displacements corrections

$$\dot{\mathbf{u}} = -\mathbf{K}^{-1}\mathbf{s}\left(\mathbf{u}_1 + \Delta\mathbf{u}, (\lambda_1 + \Delta\lambda + \dot{\lambda})\bar{\mathbf{u}}\right), \tag{9}$$

where the tangent stiffness matrix related to the free displacements $\mathbf{K}$ is computed for $\mathbf{u} + \Delta\mathbf{u}$.

In order to make equal the number of equations to those of unknowns, we have to write one more equation which expresses the imposed constraint. A suitable, and general, form for this constraint is the following:

$$\Delta\mathbf{u}^T\mathbf{C}\dot{\mathbf{u}} + \gamma\Delta\lambda\dot{\lambda} = 0, \tag{10}$$

where the matrix $\mathbf{C}$ and the scalar γ can to be opportunely chosen in order, for example, to accelerate the convergence or to simplify the necessary calculations. We stress that the condition (10) is rather general and can be interpreted as a sort of orthogonality condition between extrapolation, i.e., the pair $(\Delta\lambda, \Delta\mathbf{u})$, and correction, i.e., the pair $(\dot{\lambda}, \dot{\mathbf{u}})$.

Straightforward calculations, using Eq. (10), allows to compute

$$\dot{\lambda} = \frac{\Delta\mathbf{u}^T\mathbf{C}\mathbf{K}^{-1}\mathbf{s}\left(\mathbf{u}_1 + \Delta\mathbf{u}, (\lambda_1 + \Delta\lambda)\bar{\mathbf{u}}\right)}{\gamma\Delta\lambda - \Delta\mathbf{u}^T\mathbf{C}\mathbf{K}^{-1}\Delta\mathbf{s}}, \tag{11}$$

where

$$\Delta\mathbf{s} = \frac{\mathbf{s}\left(\mathbf{u} + \Delta\mathbf{u}, (\lambda + \Delta\lambda + \tilde{\lambda})\bar{\mathbf{u}}\right) - \mathbf{s}\left(\mathbf{u} + \Delta\mathbf{u}, (\lambda + \Delta\lambda)\bar{\mathbf{u}}\right)}{\tilde{\lambda}}. \tag{12}$$

Now, in order to obtain a specific algorithm, we have to select $\mathbf{C}$ and γ. A desirable choice is the pair $\mathbf{C} = \mathbf{K}$ and $\gamma = 0$ since it produces a simple expression for the correction. In formula, the corresponding expression for $\dot{\lambda}$ becomes

$$\dot{\lambda} = -\frac{\Delta\mathbf{u}^T \mathbf{s}\,(\mathbf{u}_1 + \Delta\mathbf{u}, (\lambda_1 + \Delta\lambda)\bar{\mathbf{u}})}{\Delta\mathbf{u}^T \Delta\mathbf{s}}, \tag{13}$$

whereas $\dot{\mathbf{u}}$ can easily be computed by using Eq. (9).

In order to complete the algorithm sketched in the immediate foregoing, it is necessary to define the first extrapolation at the beginning of each step. The simplest way is to define it on the basis of the previous steps. Using the terminology already introduced, we can compute

$$\begin{aligned} \Delta\lambda &= m(\lambda_1 - \lambda_0), \\ \Delta\mathbf{u} &= m(\mathbf{u}_1 - \mathbf{u}_0), \end{aligned} \tag{14}$$

where the coefficient m is tailored to modify the arc-length during the step-by-step procedure: increasing the step-length in the part of the curve which does not present particular problem (weakly nonlinear), and decreasing it in the part of the curve which require more care (strongly nonlinear). A simple formula for the coefficient m is given as

$$m = 1 - \frac{r_l - n_l}{r_l + n_l}, \tag{15}$$

and it is able to modify the arc-length on the basis of the number of required r_l and needed n_l loops necessary to reach the convergence of the scheme. At the first step, we can set $m = 1$ and fix the value of $\Delta\lambda$, defining implicitly the desired arc-length, and compute the corresponding value of $\Delta\mathbf{u}$.

3 Experimental results and parameter identification

We assume here that all the corresponding structural elements constituting the substructures used in the experiments are identical in their mechanical and geometrical properties. This can be confirmed by the visual measurements performed on the specimens before and after rupture. Furthermore, the repeatability of the results obtained with different specimens and the authors' experience with the 3D printing process confirm this assumption.

The considered substructures have 7 pivots, four of which have, in considered measurements, exactly the same mechanical role (see Fig. 7). These pivots are those placed at the external free nodes of the pantograph (nodes 4, 5, 7 and 8). The central pivot, node 6, is the one which is twisted the most and the two remaining pivots, 3 and 9, have the twist angle partially blocked by the clamping of the extremities of interconnected beams.

The beam segment of fibers are undergoing large displacements and deformations and a fully nonlinear description of their mechanical behavior is demanded. The parameters to be identified are therefore:

(i) those characterizing the micro-twist (that is the macro-shear) at the interconnecting pivots;
(ii) those characterizing the bending of the beam segment of fibers, distinguished into interconnecting nodal and intermediate nodal rotational stiffnesses;
(iii) those characterizing the extension of the beam segment of fibers.

We start by assuming that the deformation energy is quadratic in the nonlinear deformation measures characterizing each introduced rotational and extensional stiffnesses. We assume the geometric data reported in Sect. 1. Furthermore, we set for the maximum displacement on one of the shorter side of the pantographic sheet, in the direction of the longer side, equal to 12 mm which is the same values adopted in the experimental test.

Four pictures of the experimental test are shown in Fig. 8 for the non-dimensional given displacement λ varying from 0, at the beginning of the test, to 1 in correspondence of the given displacement of 12 mm.

During the physical experiment, the reaction force R was measured corresponding to the given displacement. Figure 9 reports, besides the measured force R, two fits using quadratic and cubic interpolation laws. The plot shows that, although cubic interpolation follows closely the experimental curve, quadratic interpolation is not so far from the cubic one.

(a) $\lambda = 0.25$

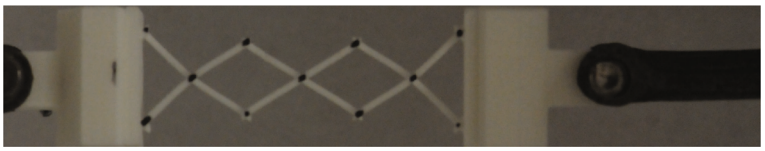

(b) $\lambda = 0.5$

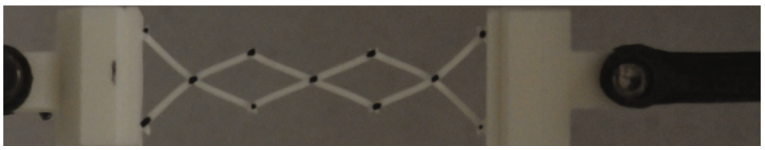

(c) $\lambda = 0.75$

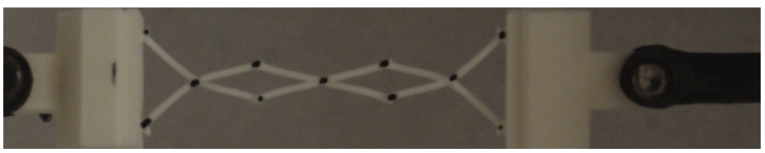

(d) $\lambda = 1$

Fig. 8 Physical experiment: deformation varying the non-dimensional given displacement parameter λ

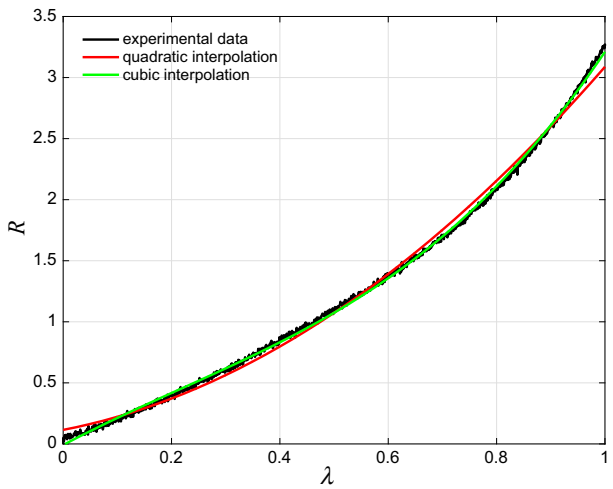

Fig. 9 Measured global structural reaction R and its fitting with a quadratic and a cubic law *vs.* non-dimensional given displacement λ

To replicate the results of the experiment reported in the foregoing, we performed a series of numerical simulations using the enhanced Piola–Hencky model described in Sect. 2. The values for the stiffness parameters necessary to completely describe the discrete model, that is a, b and s for axial, bending and shearing stiffness, respectively, have to be properly identified in order to follow closely the results of the experiment: in practice, the deformations for one or more fixed value of λ and/or the force–displacement curve.

As first estimate, we considered the stiffnesses deriving from the De Saint Venant problem (which are rigorously valid only for the linear case). In formulae

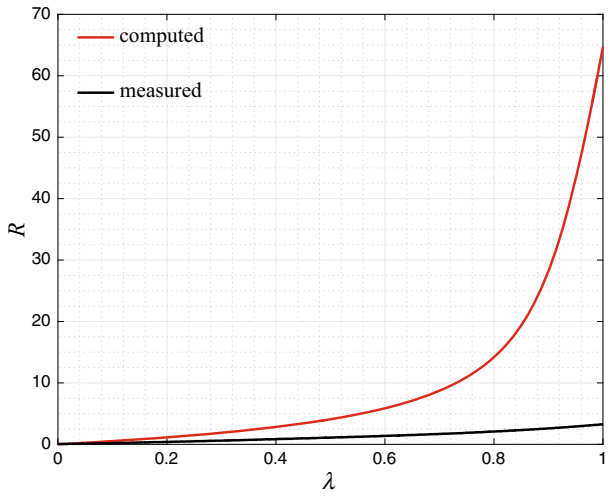

Fig. 10 Comparison for the computed and measured global force R obtained estimating a, b and s from $Y = 1700$ MPa

$$\begin{aligned} a &= \frac{YA}{\ell}, \\ b &= \left(1 - \frac{\ell}{L}\right)\frac{YI}{\ell}, \\ 4s &= \frac{GI_p}{\ell_p}, \end{aligned} \tag{16}$$

where Y and G are the Young's and the shear moduli of the polyamide, respectively; A and I are the area and the inertia of the cross section, L the total length of the micro-beam, and ℓ is the length of each one of the segment of the micro-beam (between two elastic joints). The coefficient $1 - \ell/L$ take into account the number of elastic joints used to model the bending strain energy.

The Young's modulus Y and the Poisson's ratio ν of the polyamide used in 3D printing process can be extracted from the technical specifications from the polyamide following EN ISO 527 which suggests $Y = 1700$ MPa and $\nu = 0.4$.[1]

Since the printing process could influence, rather significantly, the constitutive parameters of the polyamide we were prepared to revise, even strongly, the initial estimates. However, we start our simulations computing an initial estimate of a, b and s using (16) with $Y = 1700$ MPa and $\nu = 0.4$. Simple calculations give $a = 369.9$ N/mm, $b = 23.12$ Nmm and $s = 4.888$ Nmm. With these values of the stiffnesses, we compute the global structural reaction $R(\lambda)$ curve. The comparison between the computed and measured curve is reported in Fig. 10.

Figure 10 shows without doubt the stiffnesses of the discrete model cannot be computed using (16) or, alternatively, that the Young's modulus is lower than the used value, i.e., 1700 MPa. For this reason, we considered the identification of the stiffness parameters of the discrete model using the methods described, for example, in [43]. The simpler way is to consider

$$\chi = \|\mathbf{x}_j - \bar{\mathbf{x}}_j\|^2 = \min \tag{17}$$

where $\mathbf{x}_j$ and $\bar{\mathbf{x}}_j$ are, for example, the position of the jth pivots computed from the numerical model and from the physical experiment, respectively, for a fixed value of λ. Alternatively, we can identify the stiffness parameters minimizing the distance from the equilibrium curve computed by means of the numerical model and from the experiment where, this time, $\mathbf{x}_j$ and $\bar{\mathbf{x}}_j$ points of the equilibrium curve computed by the numerical simulation and from the experiment.

A first attempt to estimate the correct value of a, b and s can be pursued scaling the three stiffnesses by the same number or, in other words, to scale the Young's modulus Y in such a way that the global structural reaction R computed and measured for $\lambda = 1$ be the same. The values of the stiffnesses which ensures this

[1] See https://www.shapeways.com/rrstatic/material_docs/mds-strongflex.pdf.

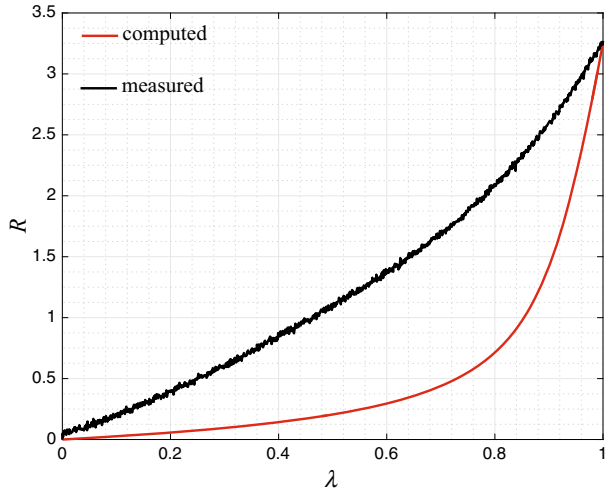

Fig. 11 Comparison for the computed and measured global force R obtained estimating a, b and s from $Y = 85.53$ MPa

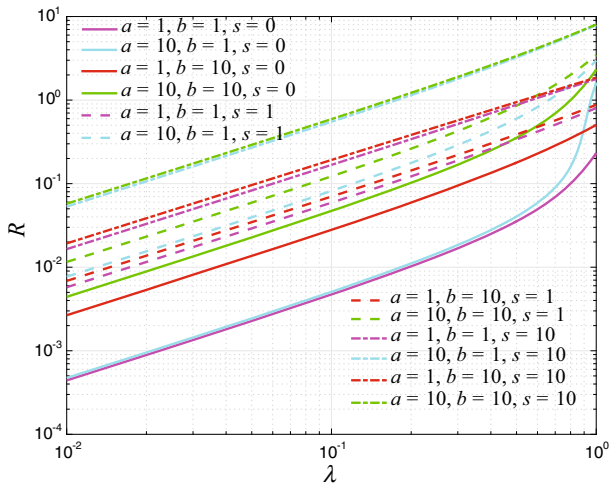

Fig. 12 Abacus to identify the stiffnesses a, b and s: global structural reaction R *vs.* the non-dimensional given displacement λ

result are $a = 18.61$ N/mm, $b = 1.163$ Nmm and $s = 0.2459$ Nmm corresponding to a Young's modulus $Y = 85.53$ MPa.

Although the global structural reaction R is now the same for $\lambda = 1$, the computed and measured curves are somewhat different and therefore the ratios among a, b and s have to be changed. This goal can be achieved by a black-box procedure which optimizes the stiffnesses to minimize the discrepancy between measured and computed curves. However, it is interesting, in itself, a simple parametric study of the $R(\lambda)$-curve varying the stiffnesses a, b and s, in other words the kind of abacus, in logarithmic scale, reported in Fig. 12. From the plots, we deduce that:

1. the value of R computed for $\lambda = 1$ is strongly related to a;
2. the stiffness b shift the plot upward leaving the slope of the first part of the graph unaltered, the slope of the second part of the curve becomes less accentuated when b increases;
3. the stiffness s, beyond to shift upward the curves (like b), makes the whole curve flat.

With the guidelines briefly depicted in the foregoing, it is simple, by using very few iterations to reach a set of stiffnesses a, b and s which produces a remarkable fitting of the experimental curve. We report in Fig. 13 the $R - \lambda$ curve obtained with the stiffnesses $a = 6.5$ N/mm, $b = 2.0$ Nmm and $s = 2.2$ Nmm which now shows a good agreement with the experimental one reported in black.

In order to show how the strain energy is split in the axial E_a, bending E_b and shear E_s parts, we report in Fig. 14 the three energy components, when λ increases, for the same set of stiffnesses.

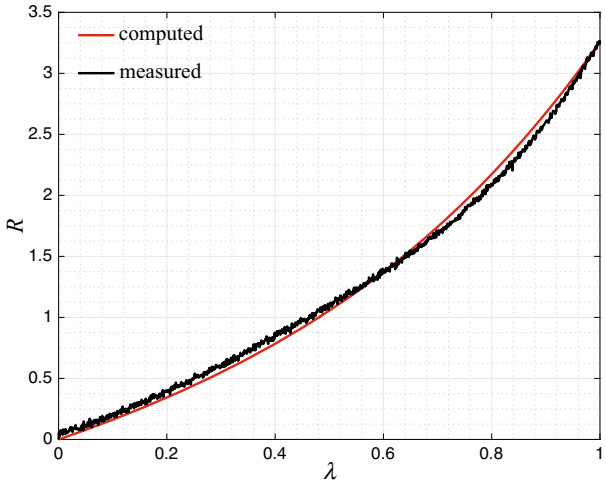

Fig. 13 Comparison between physical experiment (in black) and numerical simulation (in red) for the global structural reaction R *vs.* the non-dimensional given displacement λ for the set $a = 6.5$ N/mm, $b = 2.0$ Nmm and $s = 2.2$ Nmm

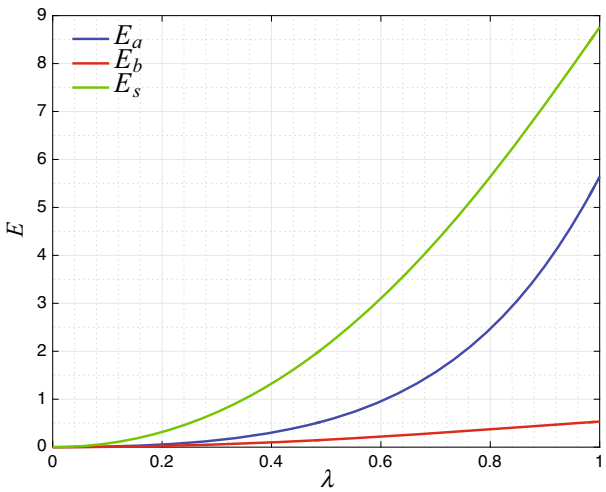

Fig. 14 Split of strain energy in its extensional E_a, bending E_b and shear E_s *vs.* the non-dimensional given displacement λ for the set $a = 6.5$ N/mm, $b = 2.0$ Nmm and $s = 2.2$ Nmm

Furthermore, Fig. 15 reports the history of the deformation for λ equal to 0.25, 0.5, 0.75 and 1. Color map describes the strain energy density on the micro-beams.

We remark that the deformations do not perfectly overlap the pictures taken during the physical experiment. More precisely, comparing the pictures shown in Fig. 8 and the numerical simulations reported in Fig. 15, it seems than the deformations corresponding to $\lambda = 0.75$ and $\lambda = 1$ in the physical experiment are more marked. Obviously, it is possible, changing the set of stiffnesses, to overlap precisely the deformation for an assigned value of λ, but in this case the fit of the $R(\lambda)$-curve becomes less accurate. This lack of accuracy in the reconstruction of the deformation could be related both to the accuracy of the experiment measurements and to the numerical model which is based on well-determined choices on the energy forms which may be not adequate to this kind of problems.

4 Concluding remarks and future challenges

In the previous sections, we sketched a methodology which could be used and also formalized to identify the constitutive parameters of a discrete model capable to predict, with a good agreement, experimental results. The choice of considering a three cell only pantographic sheet was illuminating since permitted to study a

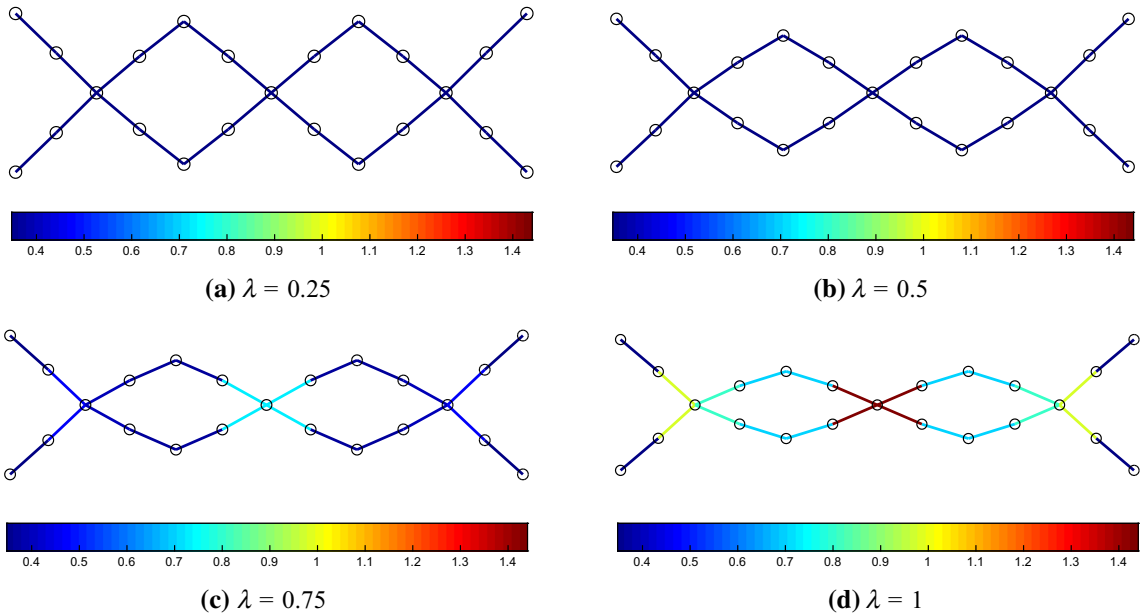

Fig. 15 History of deformation for the set of stiffnesses $a = 6.5$ N/mm, $b = 2.0$ Nmm and $s = 2.2$ Nmm for different value of the non-dimensional given displacement λ (color map shows the strain energy density level)

very simple problem and to reach some guidelines that can be used in a fruitful way to analyze more complex problems. In addition, we stress that the results obtained by using the identification procedure tuned for the enhanced Piola–Hencky numerical model could be transferred to pantographic sheets analyzed by using continuum models such as reported in [9].

Finally, we report in the list below some future challenges:

1. we only considered the elastic regime, this could be a straightjacket in the case of repeated cyclic loading process that has to be removed introducing some rate dependent constitutive equations and corresponding extra constitutive parameters;
2. even if the experimental set up has very high performances, its elongation is insufficient to achieve rupture see [44]); we will change the geometry of the pantographic substructure, for instance changing the fibers' angle, in order to lead to rupture the specimens in the available range of imposed displacements; similarly we can change the beam spacing or the beam sections;
3. up to now we considered the stiffnesses of the enhanced Piola–Hencky model invariable on the whole pantographic sheet; this hypothesis could be removed without particular computational costs to consider the study of pantographic sheet with defects, see the attempt reported in [45], or for trying to optimize the stiffnesses of the parts, micro-beams and pivots, which constitute the pantographic sheets;
4. some technical applications clearly require the extension of this study to the dynamic case since the hypothesis of quasi-static application of external loads or given displacements is no longer enough to describe some kind of behavior, see [46,47] for a prime on this topic;
5. in some discussions, initiated during Euromech Colloquia 562 and 563, see [48,49] and continued in many informal meeting and workshop organized in M&MOCS Center,[2] the following conjecture has been stated: also the problems formulated by means of discrete Hencky-type mechanical models can exploit advanced interpolation techniques. In particular, it seems suggestive and promising the adaptation of B-splines and NURBS interpolation methods. To our knowledge, the first occurrence in computational mechanics of the methods of B-splines was in [50]; however, the theory of B-splines has been incorporated in the theory of NURBS and the most popular references for these methods are [51,52]. On the other hand, the peculiar method developed in [53,54] seem to us most appropriate in the application which we have in mind;
6. the revival of Piola–Hencky-type models suggests that a revisitation of the method of statistical mechanics could be very fruitful. We are aware of the fact that in statistical mechanics, a crucial role is played by temperature. Of course, this is not the case in the mechanical systems we are studying here. However,

[2] http://memocs.univaq.it/?page_id=154 and M&moCS Youtube Channel.

already Piola, see [10,55] considered Hencky-type discrete models as a fundamental microscopic model from which generalized continua could be deduced. The methods of Piola were based on the assumption that molecules or material particles had dimensions much larger that true atoms (in the sense of Avogadro). This seems to be the multi-scale situations in which we find ourselves in the present context. The adapted methods of statistical mechanics (also for modeling foams) seem to be already available, and we hope to be able to use them in future developments [56–58];

7. peridynamics, the newly developed continuum mechanics formulation, can also be considered as an alternative approach for the analysis of pantographic sheets, see,e.g., or [59,60].

Acknowledgements Anil Misra is partly supported by United States National Science Foundation Grant CMMI-1727433.

References

1. dell'Isola, F., Lekszycki, T., Pawlikowski, M., Grygoruk, R., Greco, L.: Designing a light fabric metamaterial being highly macroscopically tough under directional extension: first experimental evidence. Zeitschrift f?r angewandte Mathematik und Physik **66**(6), 3473–3498 (2015)
2. dell'Isola, F., Della Corte, A., Greco, L., Luongo, A., Luongo, A.: Plane bias extension test for a continuum with two inextensible families of fibers: a variational treatment with lagrange multipliers and a perturbation solution. Int. J. Solids Struct. **81**, 1–12 (2016)
3. dell'Isola, F., Cuomo, M., Greco, L., Della, A.: Corte. Bias extension test for pantographic sheets: numerical simulations based on second gradient shear energies. J. Eng. Math. (2016). https://doi.org/10.1007/s10665-016-9865-7
4. Steigmann, D.J., Pipkin, A.C.: Equilibrium of elastic nets. Philos. Trans. R. Soc. Lond. A Math. Phys. Eng. Sci. **335**(1639), 419–454 (1991)
5. dell'Isola, F., Steigmann, D.: A two-dimensional gradient-elasticity theory for woven fabrics. J. Elast. **118**(1), 113–125 (2015)
6. Spagnuolo, M., Barcz, K., Pfaff, A., dell'Isola, F., Franciosi, P.: Qualitative pivot damage analysis in aluminum printed pantographic sheets: numerics and experiments. Mech. Res. Commun. **83**, 47–52 (2017)
7. Harrison, P.: Modelling the forming mechanics of engineering fabrics using a mutually constrained pantographic beam and membrane mesh. Compos. Part A Appl. Sci. Manuf. **81**, 145–157 (2016)
8. dell'Isola, F., Giorgio, I., Pawlikowski, M., Rizzi, N.L.: Large deformations of planar extensible beams and pantographic lattices: Heuristic homogenisation, experimental and numerical examples of equilibrium. Proc. R. Soc. Lond. A Math. Phys. Eng. Sci. **472**(2185), 20150790 (2016)
9. Giorgio, I., Rizzi, N.L., Turco, E.: Continuum modelling of pantographic sheets for out-of-plane bifurcation and vibrational analysis. Proc. R. Soc. A Math. Phys. Eng. Sci. **473**, 20170636 (2017)
10. dell'Isola, F., Andreaus, U., Placidi, L.: At the origins and in the vanguard of peridynamics, non-local and higher-gradient continuum mechanics: an underestimated and still topical contribution of Gabrio Piola. Math. Mech. Solids **20**(8), 887–928 (2015)
11. Alibert, J.-J., Seppecher, P., dell'Isola, F.: Truss modular beams with deformation energy depending on higher displacement gradients. Math. Mech. Solids **8**(1), 51–73 (2003)
12. Alibert, J.-J., Della, A.: Corte. Second-gradient continua as homogenized limit of pantographic microstructured plates: a rigorous proof. Zeitschrift f?r Angewandte Mathematik und Physik **66**(5), 2855–2870 (2015)
13. Carcaterra, A., dell'Isola, F., Esposito, R., Pulvirenti, M.: Macroscopic description of microscopically strongly inhomogenous systems: A mathematical basis for the synthesis of higher gradients metamaterials. Arch. Ration. Mech. Anal. **218**(3), 1239–1262 (2015)
14. Pideri, C., Seppecher, P.: A second gradient material resulting from the homogenization of an heterogeneous linear elastic medium. Contin. Mech. Thermodyn. **9**(5), 241–257 (1997)
15. Javili, A., dell'Isola, F., Steinmann, P.: Geometrically nonlinear higher-gradient elasticity with energetic boundaries. J. Mech. Phys. Solids **61**(12), 2381–2401 (2013)
16. Bertram, A.: Finite gradient elasticity and plasticity: a constitutive finite gradient elasticity and plasticity: a constitutive thermodynamical framework. Contin. Mech. Thermodyn. **28**, 869–883 (2016)
17. Auffray, N., dell'Isola, F., Eremeyev, V.A., Madeo, A., Rosi, G.: Analytical continuum mechanics ? la Hamilton-Piola least action principle for second gradient continua and capillary fluids. Math. Mech. Solids **20**(4), 375–417 (2015)
18. Greco, L., Giorgio, I., Battista, A.: In plane shear and bending for first gradient inextensible pantographic sheets: numerical study of deformed shapes and global constraint reactions. Math. Mech. Solids **22**(10), 1950–1975 (2017)
19. Eremeyev, V.A., dell'Isola, F., Boutin, C., Steigmann, D.: Linear pantographic sheets: existence and uniqueness of weak solutions. J. Elast. **2017**, 1–22 (2017)
20. Eremeyev, V.A., Pietraszkiewicz, W.: Material symmetry group and constitutive equations of micropolar anisotropic elastic solids. Math. Mech. Solids **21**(2), 210–221 (2016)
21. Bertram, A., Gl?ge, R.: Gradient materials with internal constraints. Math. Mech. Complex Syst. **4**(1), 1–15 (2016)
22. Milton, G., Briane, M., Harutyunyan, D.: On the possible effective elasticity tensors of 2-dimensional and 3-dimensional printed materials. Math. Mech. Complex Syst. **5**(1), 41–94 (2017)
23. Chatzigeorgiou, G., Javili, A., Steinmann, P.: Multiscale modelling for composites with energetic interfaces at the micro- or nanoscale. Math. Mech.Solids **20**(9), 1130–1145 (2015)
24. Misra, A., Poorsolhjouy, P.: Granular micromechanics based micromorphic model predicts frequency band gaps. Contin. Mech. Thermodyn. **28**(1), 215–234 (2016)

25. Misra, A., Poorsolhjouy, P.: Grain- and macro-scale kinematics for granular micromechanics based small deformation micromorphic continuum model. Mech. Res. Commun. **81**, 1–6 (2017)
26. Khakalo, S., Niiranen, J.: Form II of Mindlin's second strain gradient theory of elasticity with a simplification: for materials and structures from nano- to macro-scales. Eur. J. Mech. A/Solids (to appear), (2018)
27. Khakalo, S., Balobanov, V., Niiranen, J.: Modelling size-dependent bending, buckling and vibrations of 2D triangular lattices by strain gradient elasticity models: applications to sandwich beams and auxetics. J. Eng. Sci. **127**, 33–52 (2018)
28. Turco, E., dell'Isola, F., Cazzani, A., Rizzi, N.L.: Hencky-type discrete model for pantographic structures: numerical comparison with second gradient continuum models. Zeitschrift f?r Angewandte Mathematik und Physik **67**(4), 1–28 (2016)
29. Turco, E., Giorgio, I., Misra, A., dell'Isola, F.: King post truss as a motif for internal structure of (meta)material with controlled properties. R. Soc. Open Sci. **4**, 171153 (2017)
30. Golaszewski, M., Grygoruk, R., Giorgio, I., Laudato, M., Di Cosmo, F.: Metamaterials with relative displacements in their microstructure: technological challenges in 3D printing, experiments and numerical predictions. Contin. Mech. Thermodyn. (to appear) (2018)
31. Turco, E., Barcz, K., Pawlikowski, M., Rizzi, N.L.: Non-standard coupled extensional and bending bias tests for planar pantographic lattices. Part I: numerical simulations. Zeitschrift f?r Angewandte Mathematik und Physik **67**(122), 1–16 (2016)
32. Turco, E., Barcz, K., Rizzi, N.L.: Non-standard coupled extensional and bending bias tests for planar pantographic lattices. Part II: comparison with experimental evidence. Zeitschrift f?r Angewandte Mathematik und Physik **67**(123), 1–16 (2016)
33. Turco, E., Golaszewski, M., Giorgio, I., D'Annibale, F.: Pantographic lattices with non-orthogonal fibres: experiments and their numerical simulations. Compos. Part B Eng. **118**, 1–14 (2017)
34. Giorgio, I.: Numerical identification procedure between a micro Cauchy model and a macro second gradient model for planar pantographic structures. Zeitschrift f?r Angewandte Mathematik und Mechanik **67**(95), 1–17 (2016)
35. Placidi, L., Andreaus, U., Della Corte, A., Lekszycki, T.: Gedanken experiments for the determination of two-dimensional linear second gradient elasticity coefficients. Zeitschrift f?r Angewandte Mathematik und Physik (ZAMP) **66**(6), 3699–3725 (2015)
36. Misra, A., Poorsolhjouy, P.: Identification of higher-order elastic constants for grain assemblies based upon granular micromechanics. Math. Mech. Complex Syst. **3**(3), 285–308 (2015)
37. Boutin, C., dell'Isola, F., Giorgio, I., Placidi, L.: Linear pantographic sheets. Asymptotic micro-macro models identification. Math. Mech. Complex Syst. **5**(2), 127–162 (2017)
38. Misra, A., Poorsolhjouy, P.: Elastic behavior of 2D grain packing modeled as micromorphic media based on granular micromechanics. J. Eng. Mech. **143**(1), C4016005 (2017)
39. Turco, E., Golaszewski, M., Cazzani, A., Rizzi, N.L.: Large deformations induced in planar pantographic sheets by loads applied on fibers: experimental validation of a discrete Lagrangian model. Mech. Res. Commun. **76**, 51–56 (2016)
40. Riks, E.: The application of Newton's method to the problem of elastic stability. J. Appl. Mech. Trans. ASME **39 Ser E**(4), 1060–1065 (1972)
41. Clarke, M.J., Hancock, G.J.: A study of incremental-iterative strategies for non-linear analyses. Int. J. Numer. Methods Eng. **29**, 1365–1391 (1990)
42. Turco, E., Caracciolo, P.: Elasto-plastic analysis of Kirchhoff plates by high simplicity finite elements. Comput. Methods Appl. Mech. Eng. **190**, 691–706 (2000)
43. Turco, E.: Tools for the numerical solution of inverse problems in structural mechanics: review and research perspectives. Eur. J. Environ. Civ. Eng. **21**(5), 509–554 (2017)
44. Turco, E., dell'Isola, F., Rizzi, N.L., Grygoruk, R., M?ller, W.H., Liebold, C.: Fiber rupture in sheared planar pantographic sheets: numerical and experimental evidence. Mech. Res. Commun. **76**, 86–90 (2016)
45. Turco, E., Rizzi, N.L.: Pantographic structures presenting statistically distributed defects: numerical investigations of the effects on deformation fields. Mech. Res. Commun. **77**, 65–69 (2016)
46. Giorgio, I., Della Corte, A., dell'Isola, F.: Dynamics of 1D nonlinear pantographic continua. Nonlinear Dyn. **88**(1), 21–31 (2017)
47. Engelbrecht, J., Berezovski, A.: Reflections on mathematical models of deformation waves in elastic microstructured solids. Math. Mech. Complex Syst. **3**(1), 43–82 (2015)
48. dell'Isola, F., Forest, S.: Second gradient and generalized continua. A workshop held on 12?16 March 2012 in Cisterna di Latina. ZAMM J. Appl. Math. Mech. /Zeitschrift f?r Angewandte Mathematik und Mechanik **94**(5), 367–372 (2014)
49. Placidi, L., Giorgio, I., Della Corte, A., Scerrato, D.: Euromech 563 Cisterna di Latina 17?21 March 2014 Generalized continua and their applications to the design of composites and metamaterials: a review of presentations and discussions. Math. Mech. Solids **22**(2), 144–157 (2017)
50. Aristodemo, M.: A high-continuity finite element model for two-dimensional elastic problems. Comput. Struct. **21**(5), 987–993 (1985)
51. Piegl, L., Tiller, W.: The NURBS Book, 2nd edn. Springer, Berlin (1997)
52. Cottrell, J.A., Hughes, T.J.R., Bazilevs, Y.: Isogeometric Analysis: Toward Integration of CAD and FEA. Wiley, Hoboken (2009)
53. Greco, L., Cuomo, M., Contraffatto, L., Gazzo, S.: An efficient blended mixed B-spline formulation for removing membrane locking in plane curved Kirchhoff rods. Comput. Methods Appl. Mech. Eng. **324**, 476–511 (2017)
54. Greco, L., Cuomo, M.: B-Spline interpolation of Kirchhoff-Love space rods. Comput. Methods Appl. Mech. Eng. **256**, 251–269 (2013)
55. dell'Isola, F., Maier, G., Perego, U., Andreaus, U., Esposito, R., Forest, S.: The complete works of Gabrio Piola: Volume I - Commented English Translation. Springer, Berlin (2014)
56. De Masi, A., Merola, I., Presutti, E., Vignaud, Y.: Potts models in the continuum uniqueness and exponential decay in the restricted ensembles. J. Stat. Phys. **133**(2), 281–345 (2008)
57. De Masi, A., Merola, I., Presutti, E., Vignaud, Y.: Coexistence of ordered and disordered phases in Potts models in the continuum. J. Stat. Phys. **134**(2), 243–306 (2009)

58. Grimmett, G.R.: Correlation inequalities for the Potts model. Math. Mech. Complex Syst. **4**(3?4), 327–334 (2016)
59. Diyaroglu, C., Oterkus, E., Oterkus, S., Madenci, E.: Peridynamics for bending of beams and plates with transverse shear deformation. Int. J. Solids Struct. **69**, 152–168 (2015)
60. De Meo, D., Diyaroglu, C., Zhu, N., Oterkus, E., Siddiq, M.A.: Modelling of stress-corrosion cracking by using peridynamics. Int. J. Hydrog. Energy **41**(15), 6593–6609 (2016)